Volume 9, Issue 6, 2019, 4629 - 4634 ISSN 2069-5837

Biointerface Research in Applied Chemistry

www.BiointerfaceResearch.com

https://doi.org/10.33263/BRIAC96.629634

Original Research Article Open Access Journal

Received: 04.10.2019 / Revised: 14.11.2019 / Accepted: 15.11.2019 / Published on-line: 20.11.2019

Temperature dependence of indentation behavior of Ti-6Al-4V alloy for bio medical applications

B Sridhar Babu [1], Kaushik Kumar [2,*]

[1]Professor, Department of Mechanical Engineering, CMR Institute of Technology, Hyderabad, India
[2]Associate Professor, Department of Mechanical Engineering, BIT Mesra, Ranchi, Jharkhand, India

*corresponding author e-mail address: ***kkumar@bitmesra.ac.in*** | Scopus ID: 8972729400

ABSTRACT

Numerical analysis of spherical indentation was carried out to study temperature dependence (300-673K) of elasto-plastic deformation behavior of Ti-6Al-4V alloy. Flow stress and strain hardening exponent 'n' were determined from load versus indenter penetration depth profiles generated through FE model using Dao's reverse analysis approach. The upward flow around the residual impression as a function of average strain, which describes the strain hardening behaviour of the alloys was also investigated. The simulated values of CF have been used to predict high strain-rate plastic flow behavior considering indentation data. It was observed that there is a good correlation between data from simulation and experimental results in the literature. The FE model developed in the current investigation can be used for simulating the flow behavior of Ti-6Al-4V alloy. The temperature dependent CF value in the fully plastic regime from the current study is approximately 2.69 against experimentally evaluated value of 2.95. Meyer's hardness is generally high due to the presence of cold layer resulting from grinding and polishing of the test specimen. Absence of such effects in simulation of spherical indentation resulted in reduced value of CF.

Keywords: *Spherical indentation; Temperature; deformation; Numerical analysis; Ti-6Al-4V; Strain Hardening; Average strain, Pileup; Sink in ;Constrain Factor;*

1. INTRODUCTION

The most commonly used material for bio-medical applications like dental implant, orthopedic implant etc. has been Titanium and titanium-based alloys because of their acceptability by human body. Among the different types of titanium alloys, Ti64 alloy exhibits two crystal structures, one is the hexagonal closed-pack [HCP] α phase and the second is the body centered cubic [BCC] β phase. At room temperature, Ti comprises 100% α phase and at 883^0C (transus temperature) it takes allotropic transformation from α to β phase. For Ti64, vanadium (V) is added to pure Ti to stabilize the β phase by decreasing the β transus temperature. Al is added to augment the β transus temperature. With 6 wt% of Al and 4 wt% Vanadium, the β transus temperature of Ti64 is 980^0C, beyond which Ti is 100% β. It can be heat treated and aged to offer excellent mechanical properties such as the high strength to high density ratio at high temperatures, which are most common in bio medical applications. Usually, higher β content leads to higher creep resistance. Ti-6Al-4V remains the most widely used, as a material with a range of appropriate properties, such as higher strength, lower modulus of elasticity, better corrosion resistance and superior biocompatibility compared to other metallic biomaterials [1]. High corrosion resistance is primarily due to the spontaneous formation of the protective passive TiO_2 film on titanium further, owing to its excellent mechanical and corrosion resistant properties, low density, undue importance has been given in the investigation of the mechanical behaviour of this alloy.

Spherical indentation has been evolved as simple and most effective method to determine various elasic-plastic properties of metallic materials. It is used as a substitute to uniaxial tension/compression tests in situations where the material is available in small volumes, small and irregular welds/their heat-affected zones and during failure analysis of newly developed alloys. Comprehensive analysis of static indentation has been carried out on low alloy steels heat-treated to four different hardness levels within the range HV314-569and on metallic materials namely Fe, steels, Cu, Al and its alloys. The indentation hardness of ductile materials is about 2.8–3.0 times their uniaxial flow stress.

The pressure required for plastic flow under indentation conditions is significantly high compared to uniaxial deformation conditions since the deformation underneath the indenter is constrained by the surrounding material, which is either elastic or rigid. The factor by which the resistance to plastic flow under indentation conditions is higher than the uniaxial flow stress is called Constraint Factor (CF). The influence of load and hardness on CF, depth of plastic-zone, upward flow or ridge around the indentation, and conversion of hardness vs. depth data in the plastic zone into a true strain- depth profile with suitable corrections was investigated [2-3]. The effect of temperature on constraint factor of Ti and Ni base super alloy under static indentation conditions were experimentally investigated.

2. MATERIALS AND METHODS

Finite element modelling. Two dimensional axi-symmetric FE model was created in ABAQUS with rigid spherical indenter as shown in Fig.7.1 to simulate the indentation of Ti64 alloy. In this model uni-axial true stress- strain curve is assumed to follow the

linear elastic-power law plastic model, The elastic and plastic properties of alloys used in the finite element simulations are tabulated in the Table 1 [4], it is very important to ensure that the dimensions of target materials are sufficiently large to simulate correctly the far-field boundary conditions. The sensitivity of finite element model domain size to far-field boundary conditions effects depends on the maximum indenter penetration depth and the geometry of indenter. The size of the specimen is 3000nm × 3000nm. And the maximum indentation depth is set to h_{max} = 1000nm for all simulations with conical indenters. R is indenter radius which is set to 500nm for all simulations with spherical indenters. Figure 1 gives the meshing details of the 2D axi-symmetric indentation model. Since indentation is a localized procedure that provides deformation near the contact surface, the main area of interest is close to the point of contact. Therefore, a continuous mesh was provided with variation from a fine mesh near the contact area to a coarse mesh near the boundaries. The mesh continuity was provided by sharing nodes between the elements. A fine mesh was used near the surface of the material in order to provide accuracy in describing the deformation behaviour and coarse mesh at the boundaries helped to minimize computational effort time. Since large strains distort the elements, changing point of contact conditions make a constant FE mesh inappropriate to capture a full indentation, leading to errors in calculations. Hence, a local adaptive meshing method was employed near the contact zone. This enables the software to re-mesh within time steps of the solution to ensure that the solution converged with accuracy. In any numerical study, the number of nodes or in other words the number of elements considered in the model has a direct influence on the results. Therefore, it is very important to conduct a mesh convergence study, in order to measure its influence and estimate the computational effort before carrying out the simulations. Since there is no closed-form analytical final solution for the present problem, it is not possible to measure the accuracy of the numerical method in absolute terms. Even though, a study of first ten loads vs. indenter penetration depth responses with increasing number of mesh elements i.e. coarse to fine mesh was carried out. Upon increasing the number of elements from 4000 to 6000 (in steps of 200) no significant change in results was observed beyond 4900 elements. Therefore, simulations were carried out with 4900 elements to reduce the computational effort.

In the present investigation the 'control displacement' method is employed, in this method displacement is given as input, which is equal to the indentation depth and for the applied displacement the reaction load (P) on the indenter is the summation of force over the contact zone along the indenter penetration direction. Hence the p-h curve is obtained. The FE model characterizes the contact friction behaviour between the contact surfaces using a friction coefficient 'μ'. The product μP, here P is the pressure between the two contacting material surfaces, gives the frictional shear stress[5-6]. The contact surfaces of materials will not slide until the shear stress across their interface equals the frictional shear stress, μP. In the present investigation, μ=0 is defined in all the models assuming there is no slip between the surfaces in contact. The indenter surface is defined as the 'master' surface since the indenter is rigid body. The top of the specimen is the 'slave' surface. The horizontal displacement of the work piece (specimen) and the indenter were fixed on symmetric boundaries and the vertical displacement was fixed on the work piece bottom. The applied boundary conditions to the axi-symmetric spherical indentation model are clearly shown in Figure 2.

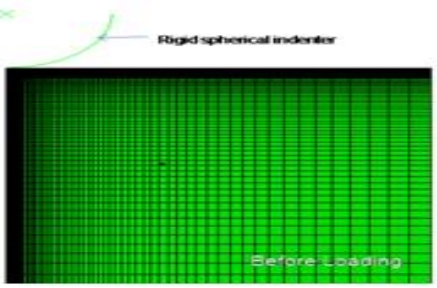

Figure 1. 2D Axi-symmetric FE model of spherical indentation before loading.

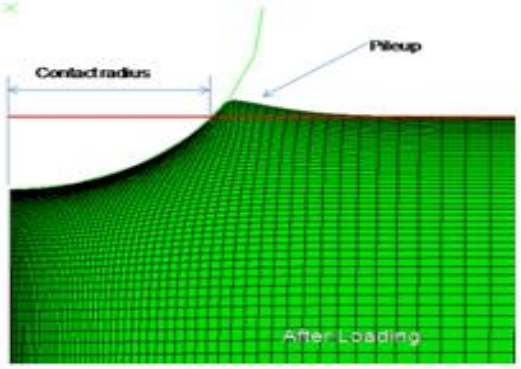

Figure 2. 2D Axi-symmetric FE model of spherical indentation after loading.

2.1. Finite Element Model Validation.

Being the computational model mainly aimed at interpreting the experimental indentation response of metallic materials, its validation was carried out by comparing the numerical and experimental results concerning the main features characterizing the indentation response, i.e. the characteristic p-*h* curve. As anticipated, the experimental indentation response of Ti64 alloy was used as the first comparison term. There exists a very good agreement between the experimental measurements and the numerical results for the material as shown in Figure 3.

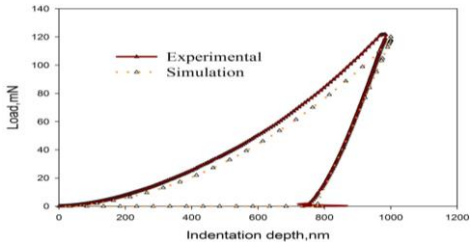

Figure 3. Comparison of experimental and simulation of Load and indentation depth curve.

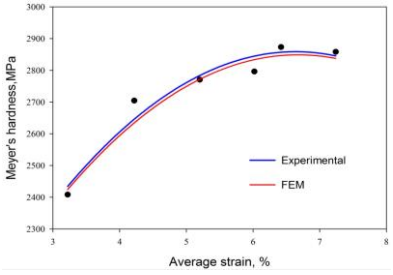

Figure 4.Comparison of experimental and simulation Mayer hardness

Data processing revealed that the relative differences between the two curves are lower than 0.5%. Meyer's hardness versus average

strain curves generated through FE analysis has been compared with the experimental curves of Ti64. It may be observed from Figure 4 that, the experimentally measured values and those extracted from simulations are correlating well.

Table.1. The input parameters of the materials at different temperatures [52].

S.No	Material	Temperature, K	Young's modulus, E (Gpa)	Poison's ratio	Strain hardening exponent, n	Strength coefficient, K, MPa
i	Ti64	300	91.91	0.23	0.08	994
ii		473	84.88	0.23	0.07	844.5
iii		673	76.67	0.23	0.07	757.3

3. RESULTS

3.1. Effect of temperature on Load and displacement curves.

The effect of temperature at indenter and specimen interface of Ti64 alloy was examined at 300K, 473K and 673K temperatures respectively. The maximum indenter penetration depth of 3mm was considered for each temperature. Figure 5 shows the p-h curve for Ti64 alloy at different temperatures. During the loading procedure, the nonlinear loading curves steadily moved upwards indicating increases in resistance of the Ti64 alloy with a decrease in the temperature and the indentation load is decreased with the increase of temperature.

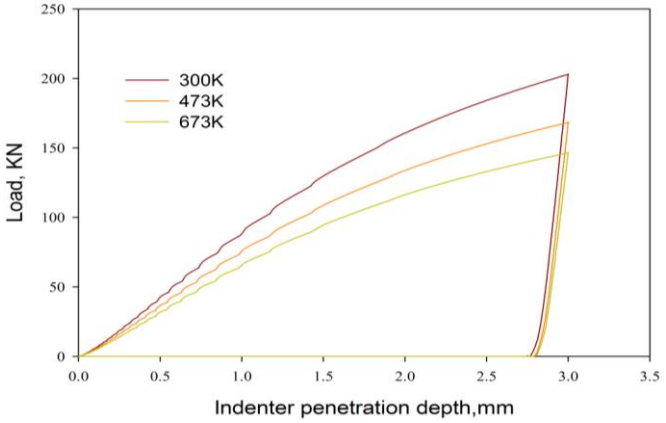

Figure 5.Variation of Load and displacement curves as a function of temperature for Ti64.

3.2. Effect of temperature on Meyer hardness.

The variation in Meyer's Hardness as a function of average strain for the Ti64 alloy is shown in Figure 6. From the finite element simulations Meyer Hardness (H_M) and average strain (ε_{av}) were determined using Dao's equations [7].

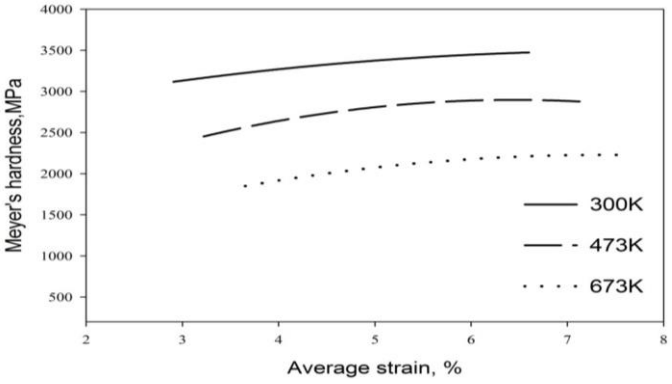

Figure 6. Meyer Hardness Vs Average strain curves at different temperatures for Ti64.

The contact area was determined by direct measurement from the simulated indentation profile at every load step. Meyer hardness was higher at room temperature and there afterward gradually decreased with an increase in temperature. The hardness was found to increase with the average strain indicating strain hardening during indentation process at all temperatures. The indentation strain hardening index 'p' was determined by analyzing Figure 6 using the Meyer's hardness relation i.e., $H_M=A\varepsilon^p$. The value of '*p'* increased from 0.15 to 0.40 with the rise in temperature from 300 to 673K, suggesting that the strain hardening gradually increased with the increase in temperature.

3.3. Effect of temperature on Young's modulus.

The Young's modulus values of Ti64 alloy was calculated at different temperatures (300-673K) using the Oliver Pharr approach[8], The variation of Young's modulus with respect to the temperature has been plotted for Ti64 alloy in Figure 7. The Young's modulus values are exhibiting significant temperature effect. The young's modulus is decreasing linearly with the increase in temperature. The decrease of Young's modulus is attributed to the change of slope in unloading curves of Ti64 alloy due to the temperature.

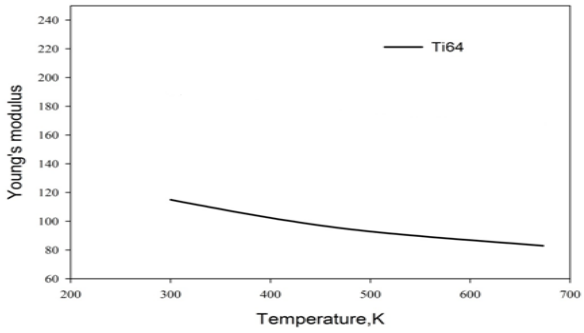

Figure 7.Variation of Youngs modulus as a function of temperature for Ti64.

3.4. Effect of temperature on the Constraint factor.

The constraint factor was computed as a function of average strain and flow stress values at different temperatures. The Constraint factor values were plotted as a function of average strain as shown in Figure 8.

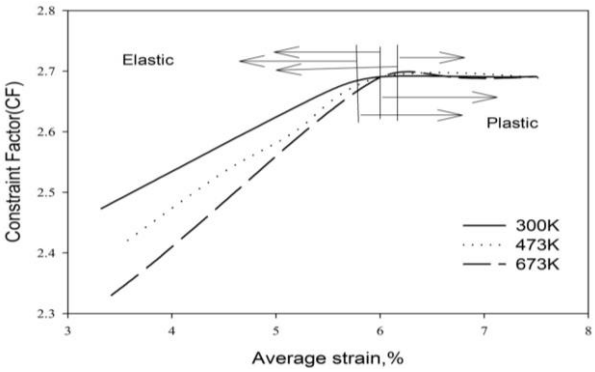

Figure 8.Variation of CF as a function of average strains at different temperatures for Ti64 alloy.

The Constraint Factor 'CF' was found to increase with increase in average strain at all temperatures up to a certain limit called transition strain, ε_{tr}, after that the constraint Factor value was found to be average strain independent. In Ti64 the fully plastic flow was observed to be at a lower strain of 4% compared

to the elevated temperatures, where transition has occurred at a strain of 6% approximately. Figure 9 shows the variation of constraint factor as a function of temperature in the elastic-plastic and plastic region. The CF is found to decrease with the increase in temperature in elastic-plastic region. However, the Constraint Factor is temperature independent in the plastic region. As per the Table.1 strain hardening index 'n' values, it is found that the' n' value is decreasing with increase in temperature; this could be the reason for the constraint factor decreasing trend in the elastic-plastic regime.

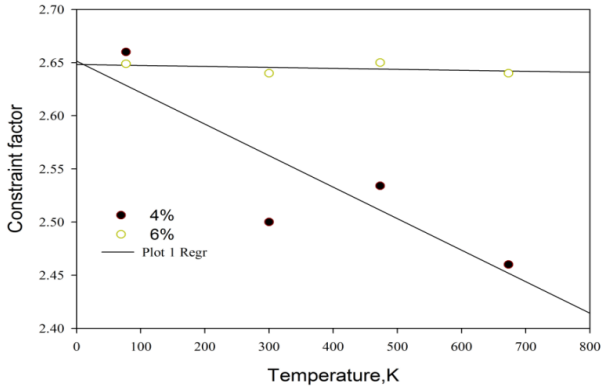

Figure 9.Variation of CF as a function of temperature at 4% and 6% true strain.

3.5. Effect of temperature on pile up and sink in behaviour.

Figure 10 shows how the pile-up behaviour depends on the temperature for Ti64 material, the indentation profiles in the loaded state were compared for three different temperatures (300K, 473K, 673K) at 3000kgf load, the height of the pile-up has been increasing with the increase in temperature. Because when the indentation depth increases the plastic zone increases and spreads outwards so pile up increases and at the small indentation depths the plastic zone decreases and the pile-up also decreases. Pile-up measured values are given in Table 2. It is known from the earlier studies by numerous investigators that, the increase in strain hardening in metallic materials decreases the pile-up around the crater. Further, higher strain hardening is known to lower the value of CF as the plastic flow of metal is accommodated well within the sample below the indenter. The above analysis reveals that, the strain hardening ability of the alloy is more predominant at elevated temperatures compared to room temperature.

Table 2. Effect of temperature and indentation load on pile-up height.

S No	Material	Pile up height, micro meters		
		300K	473K	673K
1	Ti64	1.5	2.3	3.0
2	H242	1.7	2.4	3.05

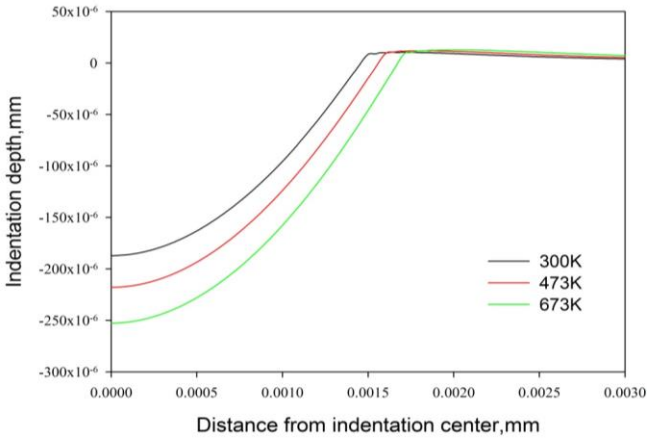

Figure 10. Indentation profiles of Ti64 alloy at different Temperatures.

3.6. Effect of temperature on strain hardening exponent and yield stress.

In the reverse analysis, the loading and the unloading response (p-h) obtained from indentation can be analyzed to derive the material plastic properties. The relation between indenter load and penetration depth during spherical indentation can be obtained by Kick's law. The values of n and σ_y were calculated using Dao's reverse analysis approach [9-10]. The calculated values of n and σ_y of Ti64 alloy were shown in Table 3 and the values are closely matched with the Finite element model input values, which were taken from the literature.

Table 3. Plastic properties of T64 and H242 alloys through reverse analysis.

S no	Temperature, K	Yield stress (MPa)	Strain hardening exponent'n'
1	300	990	0.09
2	473	780	0.08
3	673	590	0.08

3.7. Comparison of constraint factor (CF) with literature.

The Constraint factor (CF) for pure metals like Iron, Al, and Cu is in general lower and lies at a value of around 2.4 as reported by Tirupataiah and Sunderrajan, 1991[11-14]. For example for steels, a value of 2.9 to 3.0 was reported by Tirupataiah and Sunderrajan, 1991. The present work indicates that the CF for Ti alloys in the fully plastic region is 2.7 and independent of temperature. In order to understand the behaviour of CF as a function of temperature, an attempt was made in the following section to compare the FE simulation data of the present study with the existing models.

3.8. Comparison of constraint factor with theoretical models.

The FE simulation data on Constraint Factor for Ti64 as a function of temperature taken from current research has been compared with Expansion Cavity Model (ECM) and Fully Plastic Model (FPM) [15-18].

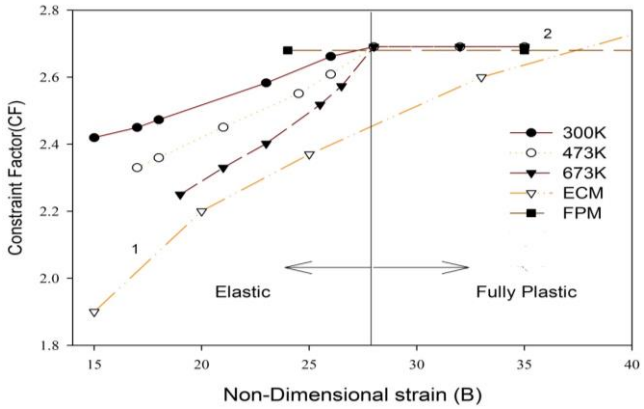

Figure 11.Comparison of Experimental constraint factor values of Ti64 with ECM and FPM theoretical models.

In Figure 11, line 1 represents Constraint Factor values calculated from the ECM considering σ_f in the place of σ_y as a function of the normalised strain 'B', line 2 represents Constraint Factor values in fully-plastic (FP) condition as given FP Model and the FE simulation data for Ti64 taken from the present work pertaining to temperatures 300K to 673K is shown in Figure 11. The Constraint Factor values of Ti64 material increased gradually with the increase in normalised strain 'B' till to a value 28,

beyond this it remained almost constant, This suggests that complete transition from elastic–plastic to fully plastic deformation occurred at a 'B' value of (28±3). This is consistent with the result obtained for metals as noted by Tirupataiah.

From the simulation data, the transition of normalized strain 'B' value was not affected by the difference in temperature. Further, the Constraint Factor was found to be independent of temperature in fully plastic region. This indicates that the change in mean pressure to cause indentation is proportional to the change in the flow stress under uniaxial compression and temperature does not affect the CF values. But it was observed that in elastic plastic regime, the Constraint Factor values at 673K were found to be lower than the values at other temperatures. As explained in section 5.2.6, the increase in strain hardening decreases the pile-up around the crater and the higher strain hardening is known to lower the Constraint Factor value or in other words, lip formation around the crater is not observed with the increase in strain hardening index. An examination of the crater profile revealed a pile-up around the crater. At 673K, neither a pile-up nor a sink-in was seen around the crater. This is an ideal case for ECM, which has an inherent assumption of the absence of pile-up and sink–in around the crater as indicated in section 5.2.6. This was probably the main reason why the cavity growth model (line1 in Fig.7.15) matches more accurately with the values obtained at temperature 673K.

4. CONCLUSIONS

The loading curves steadily shifted downwards and the maximum indentation load was decreased indicating a decrease in the resistance of the test materials with the increase in temperature.

The indentation strain hardening exponent increased with the rise in temperature from 300 to 673K, indicating that, the strain hardening gradually increased with the increase in temperature. Further, there was a drop in value of pileup around the indentation from room temperature to elevated temperatures, which is in consistence with the behavior of metallic materials.

The temperature independent CF value in the fully plastic regime from the current study is approximately 2.69 against the experimentally evaluated value of 2.95. The experimental value of Meyer's hardness is generally high due to the presence of cold layer resulting from grinding and polishing of the test specimen. Absence of such effects in simulation of spherical indentation resulted in reduced value of CF.

Decreasing trend of constraint factor in the elastic-plastic regime may be due to decreasing value of strain hardening index with the increase in temperature.

The expanding cavity model by Johnson and fully plastic model by Richmond et al, predictions are not in good agreement with FE simulation data for Ti64 up to 473K where the pile up around the crater was observed. However the data at 673K are in good agreement with the above models.

Pile-up formation has been decreasing with the increase of coefficient of fiction between indenter and material.

5. REFERENCES

1. Lee, J.H.; Kim, T.; Lee, H. A study on robust indentation techniques to evaluate elastic–plastic properties of metals. *International Journal of Solids and Structures* **2010**, *47*, 647–664, https://doi.org/10.1016/j.ijsolstr.2009.11.003.
2. Donohue, B.R.; Ambrus, A.; Kalidindi, S.R. Critical evaluation of the indentation data analyses methods for the extraction of isotropic uniaxial mechanical properties using finite element models. *Acta Materialia* **2012**, *60*, 3943–3952, https://doi.org/10.1016/j.actamat.2012.03.034.
3. Barbadikar, D.R.; Ballal, A.R.; Peshwe, D.R.; Mathew, M.D. Finite element analysis of deformation due to ball indentation and evaluation of tensile properties of tempered P92 steel. *Metallurgical and Materials Transactions A: Physical Metallurgy and Materials Science* **2015**, *46*, 3448–3459, https://doi.org/10.1007/s11661-015-2974-5.
4. Vasudeva, R.V.; Kumaraswamy, A. High strain-rate flow behavior of Ti-6Al-4V from dynamic indentation experiments. *Materials Science and Engineering-A* **2011**, *528*, 1238-1241, https://doi.org/10.1016/j.msea.2010.10.008.
5. Dean, J.; Clyne, T.W. Extraction of plasticity parameters from a single test using a spherical indenter and FEM modelling. *Mechanics of Materials* **2018**, *105*, 112–122, https://doi.org/10.1016/j.mechmat.2016.11.014.
6. Karthik, V.; Visweswaran, P.; Bhushan, A.; Pawaskar, D.N.; Kasiviswanathan, K.V.; Jayakumar, T.; Raj, B. Finite element analysis of spherical indentation to study pileup/sink-in phenomena in steels and experimental validation. *International Journal of Mechanical Sciences* **2012**, *54*, 74–83, https://doi.org/10.1016/j.ijmecsci.2011.09.009.
7. Brammer, P.; Hernot, X.; Mauvoisin, G.; Bartier, O.; Sablin. S.S. A method to take account of the geometrical imperfections of quasi-spherical indenters. *Materials and Design* **2013**, *49*, 406–413, https://doi.org/10.1016/j.matdes.2013.01.028.
8. Moussa, C.; Bartier, O.; Mauvoisin, G.; Pilvin, P.; Delattre, G. Characterization of homogenous and plastically graded materials with spherical indentation and inverse analysis. *Journal of Materials and Research* **2012**, *27*, 20-27, https://doi.org/10.1557/jmr.2011.303.
9. Sridhar, B.B.; Kumaraswamy, A.; Prasad, B.A. Investigation of Elasto–plastic deformation behavior of Hyanes 242 alloy subjected to nanoscale loads through indentation experiments. *Transaction of Indian institute of metals (Springer)* **2014,** https://doi.org/10.1007/s12666-015-0550-8.
10. Kumaraswamy, A.; Vasudeva, R.V. Effect of temperature on constraint factor of IN718 under static indentation conditions. *Materials Science and Engineering-A* **2010**, *527*, 6230-6234, https://doi.org/10.1016/j.msea.2010.06.034.
11. Sundararajan, G.; Tirupataiah, Y. The localization of plasticflow under dynamic indentation conditions: I. Experimental results. *Acta Mater.* **2006**, *54*, 565-570, https://doi.org/10.1016/j.actamat.2005.09.022.
12. Biswas, A.; Dutta, M.J. Surface characterization and mechanical property evaluation of thermally oxidized Ti–6Al–4V. *Mater Charact* **2009**, *60*, 513–518, https://doi.org/10.1016/j.matchar.2008.12.014.
13. Dean, J. & Clyne, T.W., Extraction of plasticity parameters from a single test using a spherical indenter and FEM modelling. *Mechanics of Materials*, **2017** 105, pp. 112–122, https://doi.org/10.1016/j.mechmat.2016.11.014.

14. S. Syngellakis, *et al.*, Finite element simulation of spherical indentation experiments *int. j. comp. meth. and exp. meas*.,**2018** 6, 749-763, http://doi.org/ 10.2495/cmem-v6-n4-749-763.
15. Guoxin Cao, Tianxiao Niu, Finite element modeling of the indentation behavior of two-dimensional materials *Acta Mech.*2019,230,1367–1376, https://doi.org/10.1007/s00707-017-2020-3.
16. Pingli, M.A.O.; Yan, X.I.N.; Ke, H.A.N.; Weiguo, J. Effects of heat treatment and Re-content on the TCP-phase in two Ni-Mo-Cr-Re super alloys. *Acta Metall Sin* **2009**, *22*, 365-372, https://doi.org/10.1016/S1006-7191(08)60110-6.
17. Eswar, P.K.; Chollacoop, N.; Ramamurty, U. Role of indenter angle on the plastic deformation underneath a sharp indenter and on representative strains: An experimental and numerical study. *Acta Mater.* **2009**, *59*, 4343–4355, https://doi.org/10.1016/j.actamat.2011.03.058.
18. Keryvin, V.; Prasad, K.E.; Gueguen, Y.; Sangleboeuf, J.C.; Ramamurty, U. Temperature dependence of mechanical properties and pressure sensitivity in metallic glasses below glass transition. *Philos. Mag.* **2008**, *88*, 1773-1780, https://doi.org/10.1080/14786430802286971.